

Nanoparticle Interactions Guided by Shape-Dependent Hydrophobic Forces

Shu Fen Tan, Sanoj Raj, Geeta Bisht, Harshini V. Annadata, Christian A. Nijhuis, Petr Král, and Utkur Mirsaidov*

Self-assembly of solvated nanoparticles (NPs) is governed by numerous competing interactions. However, relatively little is known about the time-dependent mechanisms through which these interactions enable and guide the nanoparticle self-assembly process. Here, using *in situ* transmission electron microscopy imaging combined with atomistic modeling, it is shown that the forces governing the self-assembly of hydrophobic nanoparticles change with the nanoparticle shapes. By comparing how gold nanospheres, nanocubes, nanorods, and nanobipyramids assemble, it is shown that the strength of the hydrophobic interactions depends on the overlap of the hydrophobic regions of the interacting nanoparticle surfaces determined by the nanoparticle shapes. Specifically, this study reveals that, in contrast to spherical nanoparticles, where van der Waals forces play an important role, hydrophobic interactions can be more relevant for nanocubes with flat side faces, where an oriented attachment between the nanocubes is promoted by these interactions. The attachment of nanocubes is observed to proceed in two distinct pathways: nanocubes either: (i) prealign their faces before the attachment, or (ii) first connect through a misaligned (edge-to-edge) attachment, followed by a postattachment alignment of their faces. These results have important implications for understanding the interaction dynamics of NPs and provide the framework for the design of future self-assembled nanomaterials.

Spontaneous bottom-up self-organization of nanoscale objects in a solution, such as biological molecules,^[1–3] inorganic, and organic nanoparticles (NPs)^[4–6] into various desired architectures is pivotal for their potential applications in catalysis,^[7] sensing,^[8] optoelectronics,^[9] and biomedicine.^[10] Since NP self-assembly in solution is governed by the competition between various interac-


tions, where individual NPs, their ligands, and solvents interact, the challenge is to identify the dominant forces driving the NP binding dynamics that determine the time-dependence and overall outcome of the self-assembly process.^[11] The NP self-assembly is driven and controlled by many competing attractive and repulsive interactions that act between the NPs, which include van der Waals (vdW) attraction, electrostatic interaction, steric repulsion, solvation forces, such as hydrophobic force, and others.^[11–13] During the self-assembly processes, attractive interactions such as vdW (between the metallic cores of NPs) and hydrophobic (between the ligated NP surfaces) forces are responsible for bringing NPs together and stabilizing them against interparticle repulsions.^[14,15]

In aqueous solutions, hydrophobic interactions between NPs (with hydrophobic surfaces) arise because the hydrogen bonding network between water molecules around the surface of each hydrophobic NP is interrupted, leading to an increase in the energy of these interfacial water molecules surrounding the NPs, which gives rise to an attractive force that drives the NP self-assembly.^[16,17] In general, hydrophobic interactions between the NPs depend on their surface properties, sizes, and shapes.^[14,18,19] During chemical synthesis, NPs are often capped with surfactant ligands to control their sizes and shapes.^[20]

Dr. S. F. Tan, G. Bisht, Prof. U. Mirsaidov
Department of Physics
National University of Singapore
Singapore 117551, Singapore
E-mail: mirsaidov@nus.edu.sg

Dr. S. F. Tan, G. Bisht, Prof. U. Mirsaidov
Centre for Bioluminescence Sciences and Department of Biological Sciences
National University of Singapore
Singapore 117557, Singapore

Dr. S. F. Tan, Prof. C. A. Nijhuis, Prof. U. Mirsaidov
Centre for Advanced 2D Materials and Graphene Research Centre
National University of Singapore
Singapore 117546, Singapore

 The ORCID identification number(s) for the author(s) of this article can be found under <https://doi.org/10.1002/adma.201707077>.

S. Raj, Prof. P. Král
Department of Chemistry
University of Illinois at Chicago
Chicago, IL 60607, USA

H. V. Annadata, Prof. C. A. Nijhuis
Department of Chemistry
National University of Singapore
Singapore 117543, Singapore
Prof. C. A. Nijhuis, Prof. U. Mirsaidov
NUSNNI-NanoCore
National University of Singapore
Singapore 117411, Singapore

Prof. P. Král
Departments of Physics and Biopharmaceutical Sciences
University of Illinois at Chicago
Chicago, IL 60607, USA

DOI: 10.1002/adma.201707077

Moreover, NPs can be further postsynthesis functionalized with various ligands to induce their specific interactions in order to direct their self-assembly.^[21–25] For example, tuning the hydrophobicity of nano-^[18] and microparticles^[26] with ligands helps to control and tailor the morphology of their colloidal assemblies.

Our current understanding of how solvent-mediated dynamic interactions drive the NP self-assembly is limited by the lack of experimental methods that allow a direct time-dependent nanoscale probing of interacting NPs in solution. Methods based on small angle X-ray scattering,^[27] UV–vis spectroscopy,^[28] and optical imaging^[29] produced much insightful information about the dynamics of NP self-assembly in solution. However, these are bulk methods, which lack the resolution needed to describe the interactions between individual NPs at different stages of the self-assembly process.

Recent advances in in situ liquid cell transmission electron microscopy (TEM)^[30–32] enable probing the interactions between NPs and their self-assembly by direct nanoscale imaging of their real-time dynamics in thin liquid films.^[33,34] This direct imaging approach has made it possible to explore how electrostatic,^[35–37] magnetic,^[38] van der Waals,^[39,40] molecular,^[41,42] capillary,^[43,44] and hydration forces^[45,46] between the NPs affect their time-dependent self-assembly.

Here, we extend this unique imaging approach to examine how shape-dependent attractive hydrophobic and vdW interactions, and repulsive electrostatic forces guide the NP self-assembly in water. We modified the NP surfaces by capping them with either a monolayer or a bilayer of cetyltrimethylammonium bromide (CTAB), an amphiphilic surfactant, by simply tuning the CTAB concentration in the solution (Section S1, Supporting Information). CTAB was chosen because it is the most commonly used cationic surfactant for NP synthesis.^[20,21,47–52] Using cuboidal gold NPs capped with a monolayer of CTA⁺, we show that hydrophobic interactions between the nanocubes (NCs) are directional, which promote their aligned face-to-face attachment, and dominate over the vdW attraction and electrostatic repulsion. We find that the strength of different attractive interactions between the NPs capped with CTA⁺ monolayers depends on the NP shape. The attractive hydrophobic forces between two NCs are greater than those between a pair of nanospheres (NSs), nanopyramids (NBPs), and nanorods (NRs) of similar sizes.

Figure 1A shows an example of the attachment of two gold NCs, each capped with a CTA⁺ monolayer, into an NC-dimer. The two gold NCs first approach each other via a translational and rotational motion, before undergoing a rapid

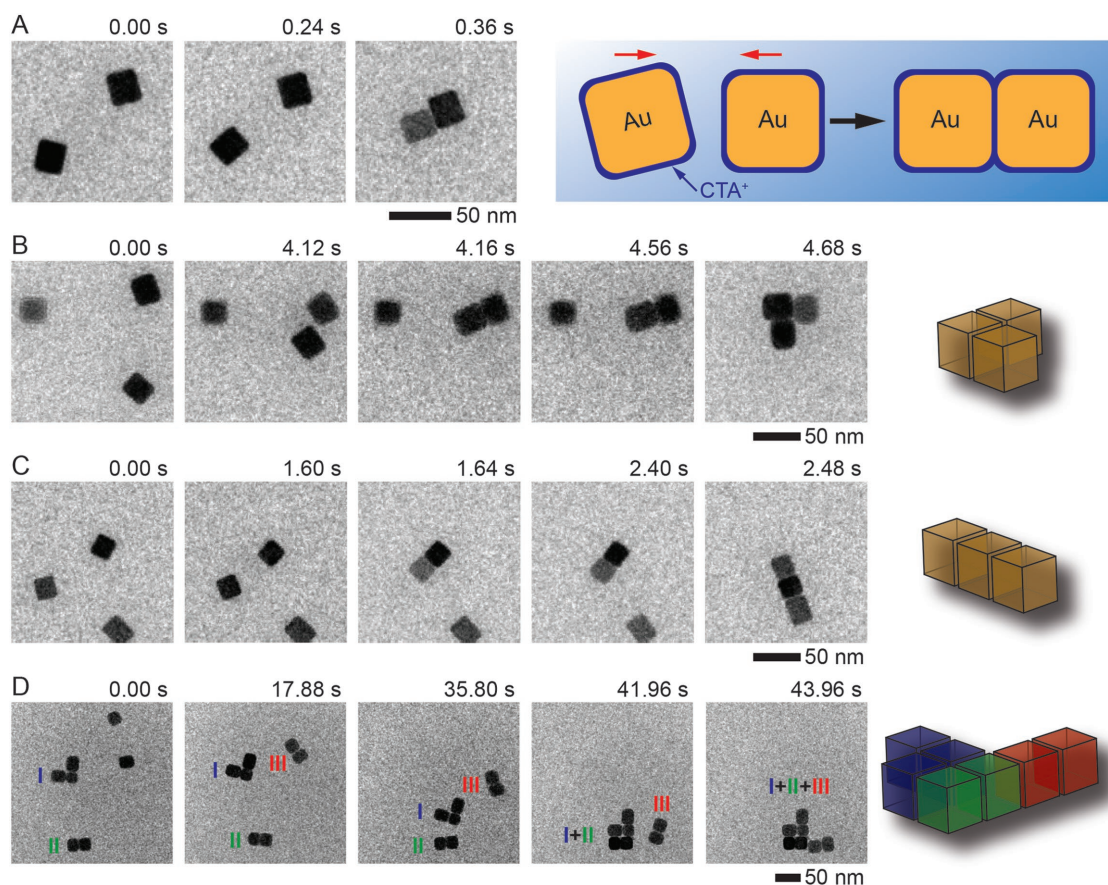


Figure 1. Pairwise interaction of CTA⁺-capped gold nanocubes in an aqueous solution. A) A time series of TEM images and a schematic showing an aligned face-to-face attachment of two gold NCs capped with CTA⁺ monolayer (Video S1, Supporting Information). A sequence of TEM images showing the attachment between three NCs into: B) an L-shaped (Video S2, Supporting Information) and C) linear NC-trimers (Video S3, Supporting Information). In both cases, all three NCs undergo the face-to-face attachment. D) TEM time-series images display the assembly of a small NC array from: I) one NC-trimer and II,III) two NC-dimer blocks (Video S4, Supporting Information).

face-to-face attachment. Similarly, in the case of three NCs, we found that the NC-trimers are formed with all their faces perfectly aligned with one another (Figure 1B,C). Furthermore, the attachment between small assembly blocks consisting of several NCs can result in larger aligned assemblies. Figure 1D shows the formation of small seven NC assembly via aligned attachment of two dimers and one trimer. In all face-to-face attachment events, we found that the postattachment spacing between the NC faces was $\approx 1\text{--}2$ nm (Section S2, Supporting Information), suggesting that the surfactant monolayers of the NCs are interdigitated and compressed upon attachment (see molecular dynamics (MD) simulations, Videos S7

and S8, Supporting Information) (the linear length of a fully stretched CTAB molecule is ≈ 2.2 nm^[53]).

Detailed examination of the attachment events reveals two distinct pathways through which NCs undergo aligned face-to-face attachments. **Figure 2A** shows the first pathway where two gold NCs move toward each other through rotational and translational movements, during which they prealign their faces, and finally attach in a face-to-face configuration. Figure 2B shows the second alternative attachment pathway where two gold NCs first attach through their edges and then rotate toward each other into a final aligned face-to-face configuration (for details of rotation dynamics see Section S3, Supporting Information). Our

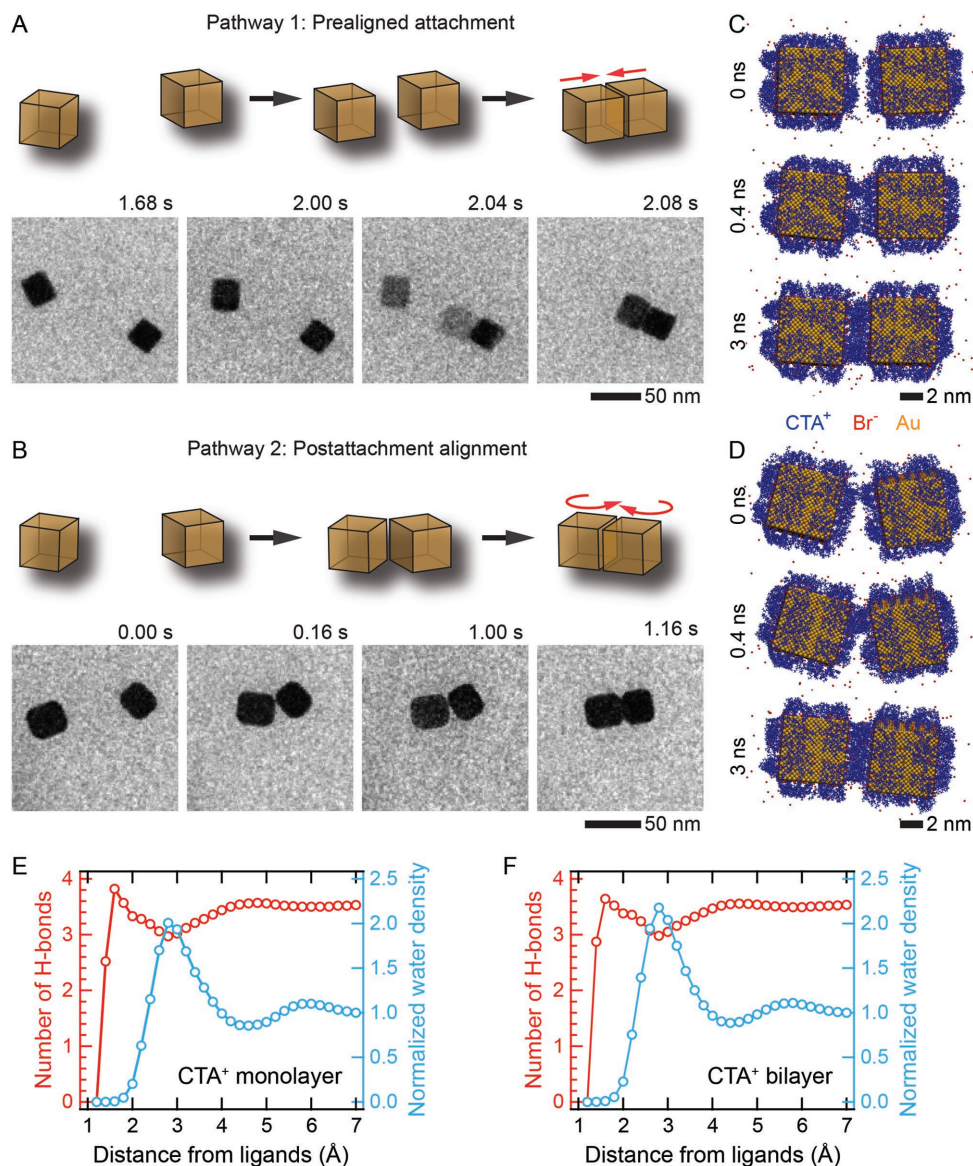


Figure 2. Face-to-face attachment of NCs in an aqueous solution. Schematics and TEM time series images showing the face-to-face attachment of two gold NCs via two pathways: A) prealigned attachment (Video S5, Supporting Information) and B) postattachment alignment of NCs (Video S6, Supporting Information). Molecular dynamics simulations showing two gold NCs (with a 5.3 nm side-length) capped with a monolayer of CTA⁺ undergoing: C) the prealigned attachment (Video S7, Supporting Information) and D) postattachment alignment (Video S8, Supporting Information). In MD simulations, gold atoms, Br⁻ counterions and cationic surfactants (CTA⁺) are represented by orange, red, and blue colors, respectively. Water molecules are omitted for clarity. The number of H-bonds per water (red) molecule and normalized water density (blue) as a function of distance from ligands for: E) a monolayer and F) a bilayer CTA⁺, capping the surface of gold NPs.

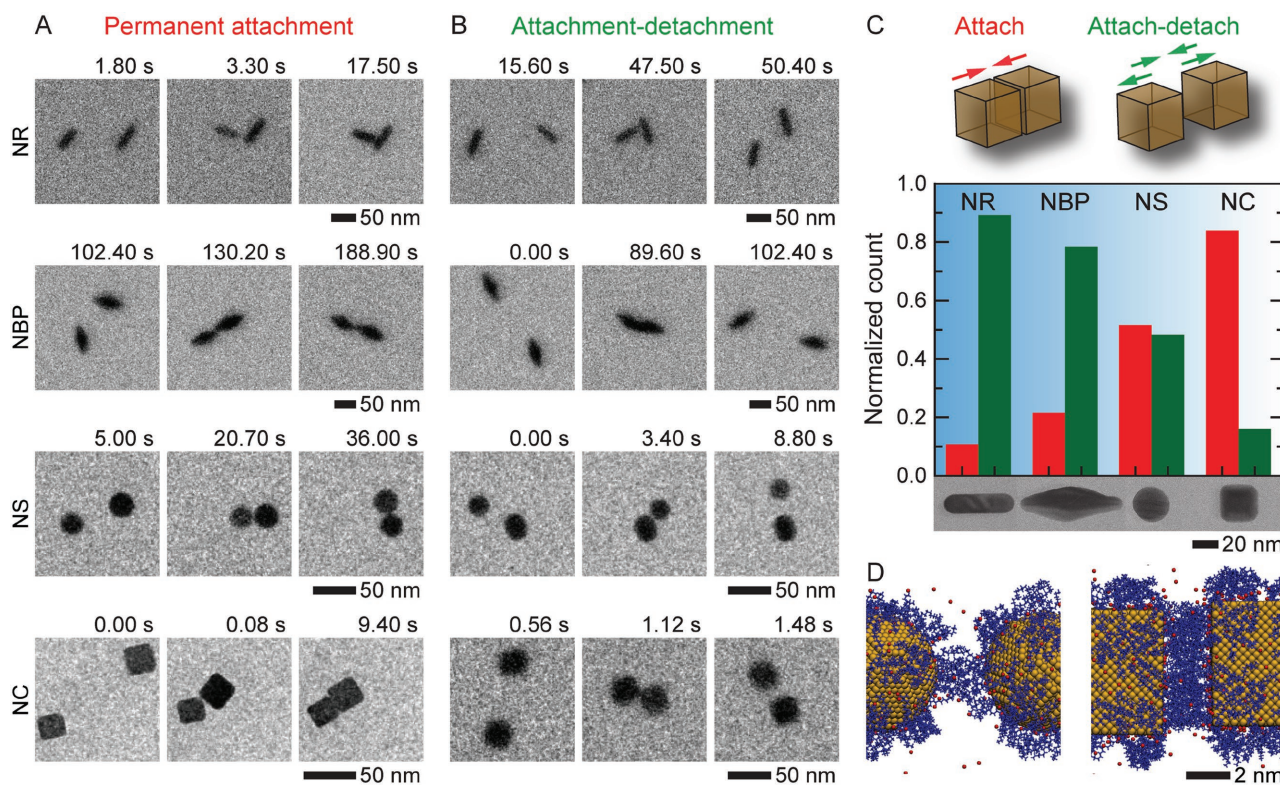


Figure 3. Interaction dynamics between NPs with different shapes. The pairwise interaction between CTA⁺-capped nanorods, nanobipyramids, nanospheres, and nanocubes results either in: A) a permanent attachment or B) a transient attachment followed by a detachment. C) The frequency of the permanent attachments (red) and postattachment detachments (green) between the NPs. The ranking of the likelihood for the permanent attachments following the pairwise contact between the NPs is NC > NS > NBP > NR. Note that, detachment of NCs is a rare event, which was observed only for NCs contacting edge-to-edge or edge-to-face. The total number of permanent and transient attachment events for NRs, NBPs, NSs, and NCs are 102, 97, 91, and 56, respectively. D) The MD simulations of pairwise attachment of NSs (left) (Video S9, Supporting Information) and NCs (right) (Video S7, Supporting Information). The overlap of CTA⁺ is greater for the attached NCs than for the NSs.

analysis of all the aligned attachment events revealed that the prealigned attachment pathway (Figure 2A) is three times more likely than the postattachment alignment pathway (Figure 2B) (Section S5, Supporting Information), suggesting that the interactions between the NCs are directional, where the face-to-face attraction is preferred. Occasionally, we also found that NCs may form assemblies with misaligned NCs when the NCs attach through their edges and fail to rotate into the aligned face-to-face configuration. This permanent misaligned attachment is most likely caused by gold–gold bonding between the NCs (Section S4, Supporting Information).

To understand the origin of the interactions between the NCs and their attachment dynamics, we modeled a system of two NCs capped with CTA⁺ monolayer in water in the presence of Br⁻ counterions using atomistic molecular dynamics simulations (Figure 2C). The Br⁻ counterions partially neutralize the 276 CTA⁺ ions in the monolayer, but the MD simulations still give a net equilibrium charge of approximately +40e for each NC, which corresponds to 236 Br⁻ ions connected to the NC. Despite a large electrostatic repulsion, these two NCs experience a significant attraction leading to their face-to-face attachment. This strong net attraction between the NCs cannot be accounted only by a gold–gold vdW force acting between their gold cores, since the CTA⁺-capped NCs carry significant charge (Section S6, Supporting Information), and the energy barrier associated with the

electrostatic repulsion between the NCs is rather large (Section S7, Supporting Information). In fact, when the simulations are repeated with the gold–gold vdW force set to 0, the NCs still undergo a pairwise attachment (Section S9, Supporting Information), which suggest that hydrophobic forces dominate during the assembly. Through simulations, we also validated the second attachment pathway. When the NCs were placed apart at an angle, they first undergo an edge-to-edge attachment, followed by their rotation into a face-to-face attachment configuration (Figure 2D). These experimental observations and simulations suggest that the hydrophobic interaction between the NC ligands may have a significant contribution to the attractive force, which leads to their attachment.

We assessed the hydrophobic coupling between the NC ligands by examining the water density and an average number of hydrogen bonds (H-bonds) per water molecule as a function of distance from the spherical NP ligands. Figure 2E shows that there is an ≈2 Å gap between the ligand and the first water layer, consistent with neutron^[54] and X-ray^[55,56] reflectivity measurements. The water density at the first water layer located 2.8 Å away from the CTA⁺ ligands is higher than the density of the bulk water (Section S10, Supporting Information). Moreover, the water molecules in the first water layer participate on average in ≈3 H-bonds, which is ≈15% less than ≈3.5 H-bonds for bulk water. In the second water

layer at 5.6 Å away from the ligands, the increase in water density and decrease in the number of H-bonds is negligible, and its contribution to the overall interaction energy should be less.

The increased water density and the loss of H-bonds in the first water monolayer surrounding the NCs cause the reduction in entropy and increase in the energy of water molecules at the ligand–water interface. The increase in free energy associated with this change in the entropy and interfacial energy (surface tension) generates attractive hydrophobic force acting between the NCs because the NC–NC attachment lowers the free energy of the system by eliminating a fraction of NCs' hydrophobic surface exposed to water (i.e., ligand–water interface). Note that for NCs capped with a CTA⁺ bilayer (in the presence of 20×10^{-3} M CTAB in solution (Section S1, Supporting Information)), a similar reduction in the number of H-bonds within the first water monolayer occurs (Figure 2F). However, owing to a much stronger electrostatic repulsion associated with the doubling of the CTA⁺ amount on the NP surfaces (Sections S6 and S9, Supporting Information), these bilayer-capped NPs repel strongly and do not come into contact (Section S8, Supporting Information). This lack of contact and attachment between the NPs is consistent with our MD simulations showing a significant repulsion between the bilayer-capped NPs (Figure S12, Supporting Information).

The preferential face-to-face attachment of NCs suggests that their cubic shape influences their pairwise hydrophobic attraction. To test how the shape of NPs, in general, affects their attraction and subsequent attachment, we also monitored the attachment of CTA⁺-capped nanospheres, nanobipyramids, and nanorods. When the CTAB concentration is $<1 \times 10^{-3}$ M, and the NPs are capped with a monolayer of CTA⁺ (Section S1, Supporting Information), NPs can attach in a solution (Figure 3A,B), but the attachments between the NPs of these shapes are weaker than the attachment between the NCs, and the once attached NPs can often detach. Figure 3C displays the frequency of permanent attachments and postattachment detachments (i.e., transient attachments). Overall, the NCs are most likely to attach permanently ($\approx 84\%$ of the cases), followed by the NSs

($\approx 52\%$) and NBPs ($\approx 22\%$), whereas the attachment between the NRs is the weakest, i.e., they detach easily (only $\approx 11\%$ of the NR–NR attachments are permanent attachments). In addition, NRs and NBPs often come into contact with their tips first because the energy barrier associated with their electrostatic repulsion is the least in the tip-to-tip configuration.^[41] However, the attachments between NBPs, which often occurs between their flat sides, as they slide sideways (Figure 3A,B), result in a permanent attachments more frequently than in the case of NRs (Figure 3C). To further confirm that similar shape-dependent trend in attachment strength persists for hydrophobic NPs capped with different hydrophobic ligand molecules, we tested the attachment dynamics between the gold NSs and between the gold NCs, both capped with thiolated-polyethylene glycol (Section S11, Supporting Information). Again, consistent with our CTA⁺-capped NPs, NSs were less likely to form permanent attachments than the NCs ($\approx 67\%$ vs $\approx 100\%$). Based on the NP shapes and sizes (Figure 3), our results suggest that the attachments with larger and larger relative surfaces result in the gradual increase in the relevance of the hydrophobic interactions in a sequence of NRs < NBPs < NSs < NCs.

The observed dependence of the attachment strength on the shape of NPs can be better explained by visualizing the overlap of CTA⁺ monolayers between the two interacting NPs. MD simulations in Figure 3D show a comparison between the attached NC-pair and NS-pair. The overlap of CTA⁺ ligands depends on the shape and the size of NPs. Here, this overlapping hydrophobic region is larger for the NCs than for the NSs because the flat surfaces of {100} gold planes (i.e., side faces of the NCs) with a strong CTA⁺ binding affinity have more overlapping CTA⁺ ligands when NPs come into a contact. Therefore, the net strength of the associated ligand-mediated hydrophobic binding is stronger for the NCs than for the NSs. Furthermore, when the vdW interaction between the NSs was set to 0 in our MD simulations, the NSs did not assemble, unlike in the case of the NCs; attachment between the NSs was possible only in the presence of both the hydrophobic and vdW attractions (Section S9, Supporting Information). This result highlights the importance of the vdW forces when other attractive interactions—in

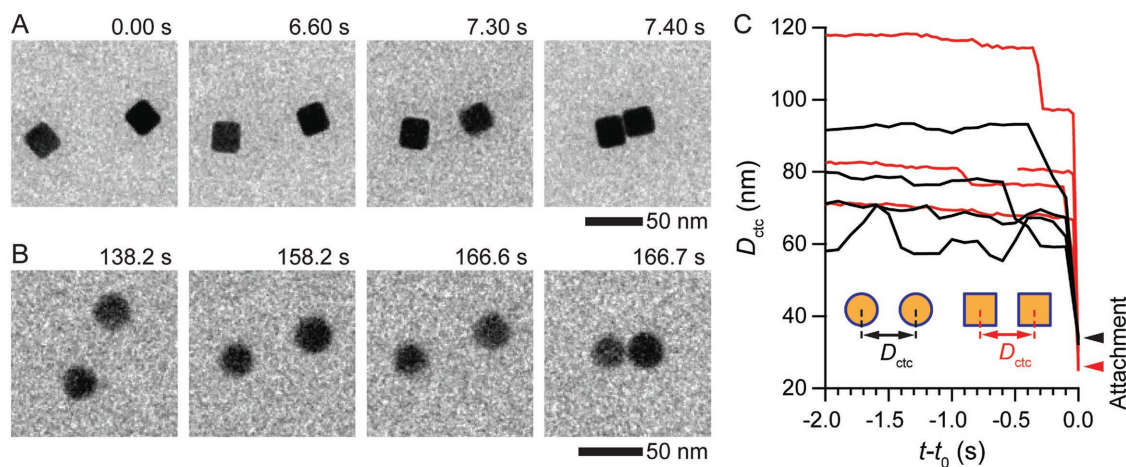


Figure 4. Long-range attractive interactions between the CTA⁺-capped NPs. A,B) A time series of TEM images showing the pairwise attachment of two CTA⁺-capped gold NCs (A) and NSs (B). C) Center-to-center separation between four gold NC pairs (red curves) and four gold NSs (black curves) similar to those shown in (A,B). Here, t_0 is the time point when the NP–NP attachments take place.

this case, hydrophobic interactions—are weak. Thus, here the shape of NPs can affect the type of the forces that drive their self-assembly. In general, since hydrophobic (overlapping hydrophobic regions) and vdW attractions also depend on NP size, both the NP size and shape determine the dominant forces responsible for NP self-assembly.

Finally, by analyzing the trajectories of interacting NPs, we found that in most attachment events the NPs jumped into contact when the separations between their surfaces were 20–100 nm (Figure 4). From the earlier studies, we expect that both vdW and hydrophobic interactions between the macroscopic surfaces to be short-range (i.e., attraction range for both of them is $\lesssim 20$ nm).^[16,57] Moreover, in those studies, long-range attractive interactions between the macroscopic surfaces were attributed to other effects, indirectly associated with surface hydrophobicity, such as a formation of bridging air nanobubbles between hydrophobic surfaces.^[17] The bridging nanobubbles were not observed in our attachment events. While our present observations alone do not allow us to directly discriminate between the vdW, hydrophobic, or other possible attractions at large separations, they suggest that the net interaction at large distances, albeit expectedly weak, is attractive and sufficient to drive the NPs into contact.

We anticipate our observations to be common to hydrophobic interactions in many nanoscopic systems. Moreover, since the size of NPs are comparable to the size of large protein complexes, these observations can stimulate studies that are important in understanding the biological processes, such as protein folding, site-specific docking, and assembly of biomolecules. In general, the ability to monitor self-assembly pathways of NPs can impact the synthesis of new materials, bottom-up nanofabrication, and structural biology.

Experimental Section

Sample Preparation: The following reagents were used to synthesize the gold NCs: gold(III) chloride trihydrate ($\text{HAuCl}_4 \cdot 3\text{H}_2\text{O}$, Cat. No. 520918, Sigma-Aldrich Co., St Louis, MO, USA), sodium borohydride (NaBH_4 , Cat. No. 213462, Sigma-Aldrich Co., St Louis, MO, USA), cetyltrimethylammonium bromide (Cat. No. 52370, Sigma-Aldrich Co., St Louis, MO, USA), copper sulfate (CuSO_4 , Cat. No. 451657, Sigma-Aldrich Co., St Louis, MO, USA), and L-ascorbic acid (Cat. No. A5960, Sigma-Aldrich Co., St Louis, MO, USA). The gold NCs with {100} face facets were synthesized using the protocol developed by Sun et al.^[58] First, a gold seed solution was prepared by reducing 6.25 mL of 1×10^{-3} M $\text{HAuCl}_4 \cdot 3\text{H}_2\text{O}$ with 150 μL of 100×10^{-3} M ice-cold aqueous solution of NaBH_4 in the presence of 18.75 mL of 100×10^{-3} M aqueous solution of CTAB, and the reaction mixture was left undisturbed for 4 h. Next, the growth solution was prepared by adding 5 mL of 2×10^{-3} M $\text{HAuCl}_4 \cdot 3\text{H}_2\text{O}$ aqueous solution into a 20 mL of 20×10^{-3} M aqueous CTAB solution. Then, into this solution, 50 μL of 10×10^{-3} M CuSO_4 aqueous solution, 3 mL of 100×10^{-3} M L-ascorbic acid, and 5 μL of gold seed solution were added sequentially. The solution was gently mixed by inversion of the test tube after the addition of each component. These synthesized NCs had a mean edge length of 24 ± 2 nm as measured from the TEM images. To test the effect of NP shape on the hydrophobic force, an aqueous suspension of CTA⁺-stabilized gold NRs (Cat. No. NR-10-750-50, Nanoseedz Ltd., Shatin, N.T., Hong Kong), CTA⁺-stabilized gold NBPs (Cat. No. NBP-20-700-20, Nanoseedz Ltd., Shatin, N.T., Hong Kong), and CTA⁺-stabilized gold NSs (Cat. No. NS-20-50, Nanoseedz Ltd., Shatin, N.T., Hong Kong) were also used.

Experimental Procedures: A 300 μL solution of the gold NPs was loaded into a 1.5 mL centrifuge tube and centrifuged twice at 10 000 rpm for 5 min and redispersed in deionized water to minimize the background CTAB concentration ($< 1 \times 10^{-3}$ M). The final working concentrations of each NP solution were as follows: $\approx 3 \times 10^{13}$ NCs mL^{-1} , $\approx 4 \times 10^{12}$ NRs mL^{-1} , $\approx 4 \times 10^{12}$ NSs mL^{-1} , and $\approx 1 \times 10^{13}$ NBPs mL^{-1} . For liquid cell experiments, ≈ 500 nL of the resulting solution was loaded into a custom microfabricated liquid cell,^[42] which is comprised of two ultrathin (≈ 20 nm) electron translucent SiN_x membranes separated by ≈ 200 nm thick spacer. Before loading the solution, these liquid cells were treated with oxygen plasma to make their SiN_x membrane surfaces hydrophilic. A Liquid Flow holder (Hummingbird Scientific, Lacy, WA, USA) and a JEOL 2010FEG TEM (JEOL Ltd, Akishima, Tokyo, Japan) operated at 200 kV for in situ TEM imaging with low electron flux ranging from 10 to 20 $\text{e} \text{ (\AA}^2 \text{ s)}^{-1}$ were used. TEM image series were acquired at a rate of 25 and 10 frames per second with an OneView CCD camera (Gatan, Inc., Pleasanton, CA, USA). The assembly of NPs was followed in real-time by observing NPs found in a $30 \mu\text{m} \times 200 \mu\text{m}$ window of the TEM liquid cell. The movies were recorded when the visible movements of the gold NPs ($t = 0$ s) were first observed.

Molecular Dynamics Simulations: CTA⁺-capped gold NCs and NSs were modeled using atomistic molecular dynamics simulations. Each gold NC had a 5.3 nm side length and was covered by 276 and 552 charged CTA⁺ molecules in the case of a monolayer and bilayer, respectively. To study the intermediate case between the monolayer and bilayer CTA⁺-capped gold NCs, another system was modeled in which 276 charged CTA⁺ molecules form the first layer, while additional 70 charged CTA⁺ molecules contribute to the partial formation of a second layer (Section S9, Supporting Information).^[59] Each gold NS had a 5.3 nm diameter and was covered by 142 and 284 charged CTA⁺ molecules in the case of a monolayer and a bilayer, respectively. Two CTA⁺-capped gold NCs and NSs were simulated in water within a $34 \times 22 \times 22 \text{ nm}^3$ box, with an appropriate number of Br^- counterions to neutralize the system. The MD simulations were performed with the Nanoscale Molecular Dynamics (NAMD) software package^[60] for an isothermal–isobaric (NPT) ensemble at $T = 300$ K, using the Langevin dynamics with a damping constant of $\gamma_{\text{Lang}} = 0.1 \text{ ps}^{-1}$ and a time step of 2 fs.

The CHARMM general force field^[61,62] was implemented for the bond, angle, and dihedral parameters of the ligands and solvent molecules. The vdW attraction and a steric repulsion, which are part of nonbonding interactions between the molecules, were described by the Lennard-Jones (LJ) potential with parameters provided by the CHARMM force field

$$U_{\text{LJ}}(r) = \epsilon \left[\left(\frac{r_{\text{min}}}{r} \right)^{12} - 2 \left(\frac{r_{\text{min}}}{r} \right)^6 \right] \quad (1)$$

Here the r^{-12} term describes an atomic repulsion because of overlapping electron orbitals, the r^{-6} term represents the vdW attractive contribution, r_{min} is a distance where $U_{\text{LJ}}(r_{\text{min}})$ has a local minimum, and ϵ is the (negative) energy at this minimum. The LJ potential implemented in NAMD has a typical cutoff distance of 1 nm (within solvent). The electrostatic interaction between charged CTA⁺ molecules, their Br^- counterions, and other partially charged atoms, which is also part of nonbonding interactions, has also a cutoff of about 1 nm. The long-range electrostatic interaction beyond the cutoff distance was calculated by the particle-mesh Ewald method^[63] in the presence of periodic boundary conditions.

The vdW interaction energy between two gold NCs was separately described by the formula^[64]

$$U(d) = -\frac{Aa^2}{12\pi} \left[\frac{1}{d^2} - \frac{2}{(d+a)^2} + \frac{1}{(d+2a)^2} \right] \quad (2)$$

and added to the CHARMM force field. Here, A is the Hamaker constant for a gold–gold interaction in water ($A = 3 \times 10^{-19}$ J), $a = 5.3$ nm is the side length of the gold NC, and d is the distance between the faces of

the gold NCs. For simplicity, the above formula was used both for the parallel and corner alignments of the cubes.

Similarly, in the case of two spherical NPs, the bulk vdW coupling between the gold cores of the NSs was separately described by the Hamaker formula^[65]

$$U(d) = -\frac{A}{12} \left(\frac{R}{d \left(1 + \frac{d}{4R}\right)} + \frac{1}{1 + \frac{d}{R} + \frac{d^2}{4R^2}} + 2 \ln \frac{d \left(1 + \frac{d}{4R}\right)}{R \left(1 + \frac{d}{R} + \frac{d^2}{4R^2}\right)} \right) \quad (3)$$

and added to the CHARMM force field. Here, $R = 2.65$ nm is the radius of the gold core, and d is the distance between the surfaces of the gold NSs.

To assess the hydrophobic coupling between NPs, the density of hydrogen bonds between the water molecules as a function of distance from the surfaces of NPs was examined. The definition of H-bond used in the calculations was based on the interaction of the O–H group of a donor water molecule with the O atom of an acceptor water molecule. Two water molecules are considered to be H-bonded when the distance between their oxygen atoms is less than 3.5 Å, and the angle between the vector joining the two oxygen atoms and the O–H bond of the donor water molecule is less than 30°. ^[66,67]

The H-bonds between the water molecules around the spherical gold NPs capped with a monolayer and bilayer of CTA⁺ ligands were analyzed. The water density and H-bond density were evaluated every 0.2 Å as a function of distance from the CTA⁺ ligands. The number of water molecules and their H-bonds in these shells defined above was calculated and averaged over 2 ns simulations.

Supporting Information

Supporting Information is available from the Wiley Online Library or from the author.

Acknowledgements

This work was supported by the Singapore Ministry of Education Academic Research Fund Tier 2 (MOE2016-T2-2-009 and MOE2015-T2-2-134), the NUS Young Investigator Award (NUSYIA-FY14-P17) from the National University of Singapore, and the NSF-DMR grant 1506886.

Conflict of Interest

The authors declare no conflict of interest.

Keywords

hydrophobic interactions, in situ transmission electron microscopy, nanoparticles, self-assembly, van der Waals forces

Received: December 4, 2017

Revised: January 14, 2018

Published online: March 14, 2018

[1] G. M. Whitesides, B. Grzybowski, *Science* **2002**, 295, 2418.

[2] S. Zhang, *Nat. Biotechnol.* **2003**, 21, 1171.

- [3] S. Zhang, D. M. Marini, W. Hwang, S. Santoso, *Curr. Opin. Chem. Biol.* **2002**, 6, 865.
- [4] Z. Nie, A. Petukhova, E. Kumacheva, *Nat. Nanotechnol.* **2010**, 5, 15.
- [5] L. Wang, L. Xu, H. Kuang, C. Xu, N. A. Kotov, *Acc. Chem. Res.* **2012**, 45, 1916.
- [6] M. Grzelczak, J. Vermant, E. M. Furst, L. M. Liz-Marzán, *ACS Nano* **2010**, 4, 3591.
- [7] G. Prieto, J. Zečević, H. Friedrich, K. P. de Jong, P. E. de Jongh, *Nat. Mater.* **2013**, 12, 34.
- [8] K. Saha, S. S. Agasti, C. Kim, X. Li, V. M. Rotello, *Chem. Rev.* **2012**, 112, 2739.
- [9] S. F. Tan, L. Wu, J. K. W. Yang, P. Bai, M. Bosman, C. A. Nijhuis, *Science* **2014**, 343, 1496.
- [10] A. E. Nel, L. Madler, D. Velegol, T. Xia, E. M. V. Hoek, P. Somasundaran, F. Klaessig, V. Castranova, M. Thompson, *Nat. Mater.* **2009**, 8, 543.
- [11] C. A. Silvera Batista, R. G. Larson, N. A. Kotov, *Science* **2015**, 350, 1242477.
- [12] Y. Min, M. Akbulut, K. Kristiansen, Y. Golan, J. Israelachvili, *Nat. Mater.* **2008**, 7, 527.
- [13] M. A. Boles, M. Engel, D. V. Talapin, *Chem. Rev.* **2016**, 116, 11220.
- [14] Z. Tang, Z. Zhang, Y. Wang, S. C. Glotzer, N. A. Kotov, *Science* **2006**, 314, 274.
- [15] A. Sánchez-Iglesias, M. Grzelczak, T. Altantzis, B. Goris, J. Pérez-Juste, S. Bals, G. Van Tendeloo, S. H. Donaldson, B. F. Chmelka, J. N. Israelachvili, L. M. Liz-Marzán, *ACS Nano* **2012**, 6, 11059.
- [16] E. E. Meyer, K. J. Rosenberg, J. Israelachvili, *Proc. Natl. Acad. Sci. USA* **2006**, 103, 15739.
- [17] W. A. Ducker, D. Mastropietro, *Curr. Opin. Colloid Interface Sci.* **2016**, 22, 51.
- [18] M. Rycenga, J. M. McLellan, Y. Xia, *Adv. Mater.* **2008**, 20, 2416.
- [19] Nie, D. Fava, M. Rubinstein, E. Kumacheva, *J. Am. Chem. Soc.* **2008**, 130, 3683.
- [20] M. Grzelczak, J. Perez-Juste, P. Mulvaney, L. M. Liz-Marzan, *Chem. Soc. Rev.* **2008**, 37, 1783.
- [21] N. D. Burrows, W. Lin, J. G. Hinman, J. M. Dennison, A. M. Vartanian, N. S. Abadeer, E. M. Grzincic, L. M. Jacob, J. Li, C. J. Murphy, *Langmuir* **2016**, 32, 9905.
- [22] M. N. O'Brien, M. R. Jones, C. A. Mirkin, *Proc. Natl. Acad. Sci. USA* **2016**, 113, 11717.
- [23] A. Dong, X. Ye, J. Chen, Y. Kang, T. Gordon, J. M. Kikkawa, C. B. Murray, *J. Am. Chem. Soc.* **2011**, 133, 998.
- [24] K. Liu, N. Zhao, E. Kumacheva, *Chem. Soc. Rev.* **2011**, 40, 656.
- [25] M. A. Boles, D. Ling, T. Hyeon, D. V. Talapin, *Nat. Mater.* **2016**, 15, 141.
- [26] Q. Chen, S. C. Bae, S. Granick, *Nature* **2011**, 469, 381.
- [27] M. C. Weidman, D.-M. Smilgies, W. A. Tisdale, *Nat. Mater.* **2016**, 15, 775.
- [28] P. K. Kundu, D. Samanta, R. Leizrowice, B. Margulis, H. Zhao, M. Börner, T. Udayabhaskararao, D. Manna, R. Klajn, *Nat. Chem.* **2015**, 7, 646.
- [29] T. P. Bigioni, X.-M. Lin, T. T. Nguyen, E. I. Corwin, T. A. Witten, H. M. Jaeger, *Nat. Mater.* **2006**, 5, 265.
- [30] M. J. Williamson, R. M. Tromp, P. M. Vereecken, R. Hull, F. M. Ross, *Nat. Mater.* **2003**, 2, 532.
- [31] H. Zheng, R. K. Smith, Y.-w. Jun, C. Kisielowski, U. Dahmen, A. P. Alivisatos, *Science* **2009**, 324, 1309.
- [32] F. M. Ross, *Science* **2015**, 350, aaa9886.
- [33] S. F. Tan, S. W. Chee, G. Lin, U. Mirsaidov, *Acc. Chem. Res.* **2017**, 50, 1303.
- [34] B. Luo, J. W. Smith, Z. Ou, Q. Chen, *Acc. Chem. Res.* **2017**, 50, 1125.
- [35] Q. Chen, H. Cho, K. Manthiram, M. Yoshida, X. Ye, A. P. Alivisatos, *ACS Cent. Sci.* **2015**, 1, 33.
- [36] J. Kim, M. R. Jones, Z. Ou, Q. Chen, *ACS Nano* **2016**, 10, 9801.

- [37] J. Kim, Z. Ou, M. R. Jones, X. Song, Q. Chen, *Nat. Commun.* **2017**, *8*, 761.
- [38] A. S. Powers, H.-G. Liao, S. N. Raja, N. D. Bronstein, A. P. Alivisatos, H. Zheng, *Nano Lett.* **2017**, *17*, 15.
- [39] T. J. Woehl, T. Prozorov, *J. Phys. Chem. C* **2015**, *119*, 21261.
- [40] E. Sutter, P. Sutter, A. V. Tkachenko, R. Krahne, J. de Graaf, M. Arciniegas, L. Manna, *Nat. Commun.* **2016**, *7*, 11213.
- [41] S. F. Tan, U. Anand, U. Mirsaidov, *ACS Nano* **2017**, *11*, 1633.
- [42] G. Lin, S. W. Chee, R. Sanoj, P. Kral, U. Mirsaidov, *ACS Nano* **2016**, *10*, 7443.
- [43] E. Miele, S. Raj, Z. Baraissov, P. Král, U. Mirsaidov, *Adv. Mater.* **2017**, *29*, 1702682.
- [44] J. Park, H. Zheng, W. C. Lee, P. L. Geissler, E. Rabani, A. P. Alivisatos, *ACS Nano* **2012**, *6*, 2078.
- [45] U. Anand, J. Lu, D. Loh, Z. Aabdin, U. Mirsaidov, *Nano Lett.* **2016**, *16*, 786.
- [46] D. A. Welch, T. J. Woehl, C. Park, R. Faller, J. E. Evans, N. D. Browning, *ACS Nano* **2016**, *10*, 181.
- [47] J. Pérez-Juste, I. Pastoriza-Santos, L. M. Liz-Marzán, P. Mulvaney, *Coord. Chem. Rev.* **2005**, *249*, 1870.
- [48] C. J. Murphy, L. B. Thompson, D. J. Chernak, J. A. Yang, S. T. Sivapalan, S. P. Boulos, J. Huang, A. M. Alkilany, P. N. Sisco, *Curr. Opin. Colloid Interface Sci.* **2011**, *16*, 128.
- [49] L. Gou, C. J. Murphy, *Nano Lett.* **2003**, *3*, 231.
- [50] S.-H. Wu, D.-H. Chen, *J. Colloid Interface Sci.* **2004**, *273*, 165.
- [51] P. Zhao, N. Li, D. Astruc, *Coord. Chem. Rev.* **2013**, *257*, 638.
- [52] D. K. Smith, B. A. Korgel, *Langmuir* **2008**, *24*, 644.
- [53] T. K. Sau, C. J. Murphy, *Langmuir* **2005**, *21*, 2923.
- [54] D. A. Doshi, E. B. Watkins, J. N. Israelachvili, J. Majewski, *Proc. Natl. Acad. Sci. USA* **2005**, *102*, 9458.
- [55] A. Poynor, L. Hong, I. K. Robinson, S. Granick, Z. Zhang, P. A. Fenter, *Phys. Rev. Lett.* **2006**, *97*, 266101.
- [56] M. Mezger, H. Reichert, S. Schöder, J. Okasinski, H. Schröder, H. Dosch, D. Palms, J. Ralston, V. Honkimäki, *Proc. Natl. Acad. Sci. USA* **2006**, *103*, 18401.
- [57] S. H. Donaldson, A. Røyne, K. Kristiansen, M. V. Rapp, S. Das, M. A. Gebbie, D. W. Lee, P. Stock, M. Valtiner, J. Israelachvili, *Langmuir* **2015**, *31*, 2051.
- [58] J. Sun, M. Guan, T. Shang, C. Gao, Z. Xu, J. Zhu, *Cryst. Growth Des.* **2008**, *8*, 906.
- [59] S. K. Meena, M. Sulpizi, *Langmuir* **2013**, *29*, 14954.
- [60] J. C. Phillips, R. Braun, W. Wang, J. Gumbart, E. Tajkhorshid, E. Villa, C. Chipot, R. D. Skeel, L. Kalé, K. Schulten, *J. Comput. Chem.* **2005**, *26*, 1781.
- [61] K. Vanommeslaeghe, E. Hatcher, C. Acharya, S. Kundu, S. Zhong, J. Shim, E. Darian, O. Guvench, P. Lopes, I. Vorobyov, A. D. Mackerell, *J. Comput. Chem.* **2010**, *31*, 671.
- [62] W. Yu, X. He, K. Vanommeslaeghe, A. D. MacKerell, *J. Comput. Chem.* **2012**, *33*, 2451.
- [63] T. Darden, D. York, L. Pedersen, *J. Chem. Phys.* **1993**, *98*, 10089.
- [64] V. Parsegian, *Van Der Waals Forces: A Handbook for Biologists, Chemists, Engineers, and Physicists*, Cambridge University Press, Cambridge, UK **2005**.
- [65] J. N. Israelachvili, *Intermolecular and Surface Forces*, 3rd ed., Academic Press, San Diego, CA **2011**.
- [66] A. Luzar, D. Chandler, *Nature* **1996**, *379*, 55.
- [67] D. Laage, J. T. Hynes, *Science* **2006**, *311*, 832.